Rock Mech Rock Engng (2009) 42: 259–288
DOI 10.1007/s00603-009-0174-6
Printed in The Netherlands

Rock Mechanics and Rock Engineering

New Viscoplastic Model for Design Analysis of Tunnels in Squeezing Conditions

By

D. Debernardi, G. Barla

Department of Structural and Geotechnical Engineering, Politecnico di Torino, Torino, Italy

Received January 16 2009; Accepted Febraury 23 2009; Published online April 17 2009

Summary

This paper is intended to describe the SHELVIP (Stress Hardening ELastic VIscous Plastic) model, a new viscoplastic constitutive law which has been developed to incorporate the most important features of behaviour observed in tunnels excavated in severe to very severe squeezing conditions. This model couples the elastoplastic and time-dependent behaviour by using a plastic yield surface, as frequently adopted in tunnel design analysis, and the definition of a state of overstress referred to a viscoplastic yield surface. The model is formulated in all its detailed aspects. The related analytical closed-form solution for representing triaxial creep deformations is developed. Also developed is an incremental numerical solution for describing the triaxial stress–strain behaviour under constant strain rate conditions. The model is shown to fit very satisfactorily the results of creep tests on clay shales and relaxation tests on coal specimens, as recently performed for design analysis of tunnels in squeezing conditions.

Keywords: Constitutive laws, squeezing conditions, time-dependent behaviour, viscoplastic behaviour, creep, relaxation

List of symbols

B	Skempton's parameter
c'	cohesion
C_{ijkl}	linear elastic deformability matrix
C_α	secondary compression coefficient
E	Young's modulus
f_p	plastic yield function

Correspondence: D. Debernardi, Department of Structural and Geotechnical Engineering, Politecnico di Torino, Torino, Italy
e-mail: daniele.debernardi@polito.it

f_{vp}	viscoplastic yield function
$f_{vp,0}$	initial value of the viscoplastic yield function
$f_{vp,0,i}$	initial value of the viscoplastic yield function for test i
$\dot{f}_p$	time derivative of the plastic yield function
$\dot{f}_{vp}$	time derivative of the viscoplastic yield function
F	overstress function
g_p	plastic potential function
g_{vp}	viscoplastic potential function
i	number of test
l	constitutive parameter
m	constitutive parameter
k_p	intercept of the Drucker-Prager's plastic yield criterion
n	constitutive parameter
p	volumetric stress
p_{ini}	volumetric component for the onset of viscoplastic deformations
$p_{ini,i}$	volumetric component for the onset of viscoplastic deformations for test i
q	deviatoric stress
q_i	deviatoric stress for test i
q_{ini}	deviatoric stress for the onset of viscoplastic deformations
$q_{ini,i}$	deviatoric stress for the onset of viscoplastic deformations for test i
s	2D mean stress
s_{ij}	stress deviator
t	time; 2D deviatoric stress
t_0	reference or initial time
W^{vp}	viscoplastic work
x	generic variable
α_p	slope of the Drucker-Prager's plastic yield criterion
α_{vp}	viscoplastic hardening level
$\alpha_{vp,0}$	initial viscoplastic hardening level
$\alpha_{vp,0,i}$	initial viscoplastic hardening level for test i
$\alpha_{vp}^{(0)}$	initial viscoplastic hardening level
$\alpha_{vp}^{(t)}$	viscoplastic hardening level at time t
$\alpha_{vp}^{(t+\Delta t)}$	viscoplastic hardening level at time $t + \Delta t$
γ	fluidity parameter
γ_i	fluidity parameter for test i
δ_{ij}	Kronecker delta
Δt	time step
$\Delta\varepsilon_a^{vp}$	axial viscoplastic strain increment
$\Delta\varepsilon_p^{vp}$	volumetric viscoplastic strain increment
$\Delta\varepsilon_q^{vp}$	deviatoric viscoplastic strain increment
$\Delta\varepsilon_r^{vp}$	radial viscoplastic strain increment
Δu	excess pore pressure
ε_a^{vp}	axial viscoplastic strain
ε_r^{vp}	radial viscoplastic strain
ε_q^{vp}	deviatoric viscoplastic strain
$\dot{\varepsilon}_a$	axial strain rate
$\dot{\varepsilon}_{ij}$	strain rate tensor
$\dot{\varepsilon}_{ij}^{e}$	elastic strain rate tensor
$\dot{\varepsilon}_{ij}^{p}$	plastic strain rate tensor
$\dot{\varepsilon}_{ij}^{vp}$	viscoplastic strain rate tensor
$\dot{\varepsilon}_a^{vp}$	axial viscoplastic strain rate
$\dot{\varepsilon}_r^{vp}$	radial viscoplastic strain rate
$\dot{\varepsilon}_a^{vp}\|_0$	axial viscoplastic strain rate for time tending to zero

$\dot{\varepsilon}_a^{vp}\big\vert_\infty$	axial viscoplastic strain rate for time tending to infinity
θ	parameter
λ	plastic multiplier
υ	Poisson's ratio
ϕ'	friction angle
Φ	viscoplastic nucleus
σ_a	axial stress
σ_r	radial stress
σ_c	consolidation effective stress
σ_{ij}	stress tensor
$\sigma_a^{(0)}$	initial axial stress
$\sigma_a^{(t)}$	axial stress at time t
$\sigma_a^{(t+\Delta t)}$	axial stress at time $t + \Delta t$
σ_t	tensile strength; volumetric tension cut-off of the Drucker-Prager's criterion
$\dot{\sigma}_a$	radial stress rate
$\dot{\sigma}_{ij}$	stress rate tensor
τ	parameter
χ	parameter
χ_i	parameter for test i
ω_p	plastic dilatancy
ω_{vp}	viscoplastic dilatancy

1. Introduction

Tunnel construction in squeezing conditions is very demanding. Difficulties are met in making reliable predictions at the design stage. During excavation squeezing is not easily anticipated, even when driving into a specific geological formation. Squeezing conditions may vary over short distances due to rock heterogeneity and changes in the mechanical and hydraulic properties of the rock mass. Indeed, the selection of the most appropriate excavation-construction method to be adopted (i.e. mechanized tunnelling versus conventional tunnelling) is highly problematic and uncertain (Barla, 2002).

Squeezing behaviour stands for large time-dependent convergence during tunnel excavation. It takes place when a particular combination of induced stresses and material properties pushes some zones around the tunnel beyond the limiting deviatoric stress at which time-dependent deformations start. It is closely related to the excavation and support techniques which are adopted. Deformations may terminate during construction or continue over a long period of time (Barla, 1995).

The consequences of squeezing consist of large tunnel closures, considerable deformations of the tunnel face, high pressures on the support, or on the shield of the Tunnel Boring Machine (TBM) in case of mechanized tunnelling, and eventually, in extreme conditions, local instabilities and collapses. Due to the fixed geometry and the limited flexibility of the TBM, allowable space to accommodate ground deformations is restricted, and the ground can slowly lock the machine (Steiner, 1996). On the contrary, in conventional tunnelling a considerably larger profile can be excavated initially in order to allow for large deformations to take place. The obvious consequence is that in deep tunnels, whenever severe squeezing conditions are anticipated, conventional tunnelling appears to be preferred over mechanized tunnelling.

In engineering practice, the difficulties to deal with squeezing conditions are connected to: (1) the evaluation of the time-dependent characteristics of the rock mass by means of laboratory or in-situ tests, (2) the use of an appropriate constitutive model,

and (3) the choice of a suitable excavation and support system. Although all these three subjects are dealt with by the Rock Mechanics and Rock Engineering group at Politecnico di Torino, this paper is intended to illustrate only the latest developments in constitutive modelling of squeezing behaviour as related to the rheologic characteristics of the solid skeleton. Therefore, the effects due to a change of pore pressure or to the alteration of the ground internal structure are neglected.

Squeezing is often represented as an equivalent elastic-plastic medium with strength and deformability parameters which are down-graded, based on observation and monitoring during excavation. The so called "short term" and "long term" conditions are often invoked, characterized by different values of the parameters involved in the constitutive model being used. However, there is no doubt that under the most severe squeezing conditions an appropriate representation of the tunnel response is obtained only by using constitutive models which account explicitly for time-dependent behaviour (Barla, 2005). This originates from the fact that time-dependent deformations are observed whenever face advancement is stopped and these are likely to take place during excavation, when it is difficult to distinguish the "face effect" from the "time effect".

Many constitutive models have been proposed in the last decades to describe the time-dependent behaviour of weak rock and soil. Nevertheless, a comprehensive bibliographic study carried out highlights that only few models can reproduce satisfactorily all the features of the time-dependent behaviour involved in tunnel excavation, with a reasonably simple mathematical formulation to be used in design practice. This observation led to the formulation of SHELVIP, a novel viscoplastic constitutive model, which is described in this paper.

The SHELVIP (Stress Hardening ELastic VIscous Plastic) model has been proposed with the intent to describe the rock mass behaviour of tunnels excavated in very severe squeezing conditions in a relatively simple, but complete manner (Debernardi, 2008). Its formulation has been based on: (1) the available experimental observations on the time-dependent behaviour of soil and weak rock, (2) the constitutive models proposed in the past, (3) the specific conditions of tunnel excavation, (4) the requirements of numerical codes and design practice, and (5) the results obtained from laboratory tests on coal specimens taken from the Carboniferous Formation and from in situ monitoring in the Saint Martin La Porte access tunnel, which experienced very important squeezing problems during excavation (Barla et al., 2007).

It is important to highlight that the version of the present SHELVIP model is currently under development and further improvements are in progress. It is expected that tertiary phase of creep and creep damage will be introduced in the near future.

2. Formulation of the SHELVIP model

The SHELVIP model couples the classical theory of elastoplasticity with a time-dependent component based on the overstress theory of Perzyna (1966). In this way, it is possible to take into account the instantaneous irreversible deformations, which are very important for tunnel excavation and, at the same time, to use a plastic law which is widely employed in design practice.

In order to maintain the constitutive model into manageable limits and to gain insights into the squeezing phenomenon, which is very complex and not yet fully

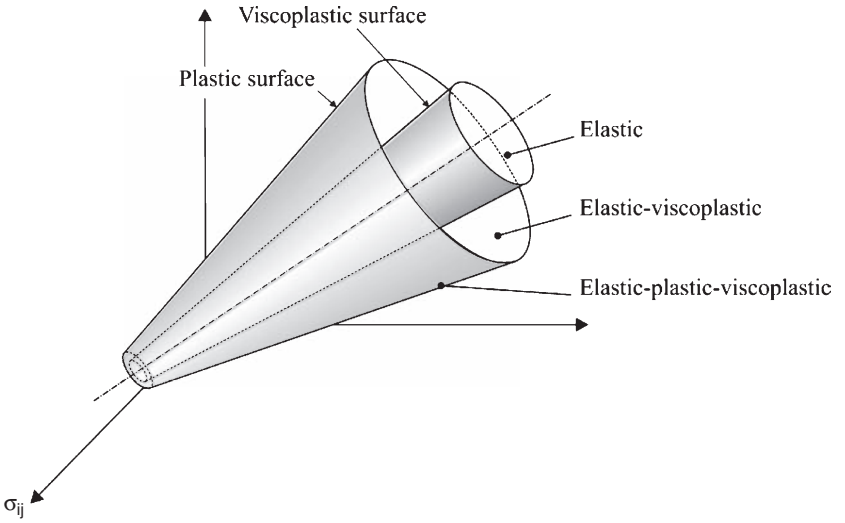

Fig. 1. Limit surfaces and stress fields in the principal stress space

understood, the following assumptions are made: an isotropic medium is considered; the pore pressure effects are taken into account only by means of Terzaghi's law (i.e. in the following all stresses are effective); dynamic and thermal effects are not considered.

The strain rate tensor $\dot{\varepsilon}_{ij}$ is divided into elastic $\dot{\varepsilon}^e_{ij}$, plastic $\dot{\varepsilon}^p_{ij}$ (time-independent), and viscoplastic $\dot{\varepsilon}^{vp}_{ij}$ (time-dependent) components, to give:

$$\dot{\varepsilon}_{ij} = \dot{\varepsilon}^e_{ij} + \dot{\varepsilon}^p_{ij} + \dot{\varepsilon}^{vp}_{ij} \tag{1}$$

In the principal stress space two limit surfaces are defined by using the Drucker-Prager's criterion: an external plastic yield surface and an internal viscoplastic yield surface (Fig. 1). The plastic yield surface defines the stress locus for onset of plastic strains according to the classical theory of elastoplasticity. The viscoplastic yield surface defines the stress threshold for development of viscoplastic strains, according to the overstress theory of Perzyna.

As illustrated in Fig. 1, the plastic and the viscoplastic yield surfaces define three different fields in the stress space:

(1) a purely elastic field inside the viscoplastic yield surface, where the deformations are only elastic, $\dot{\varepsilon}_{ij} = \dot{\varepsilon}^e_{ij}$;
(2) an elastic-viscoplastic field between the viscoplastic yield surface and the plastic yield surface, where the deformations are elastic and viscoplastic, $\dot{\varepsilon}_{ij} = \dot{\varepsilon}^e_{ij} + \dot{\varepsilon}^{vp}_{ij}$;
(3) an elastic-plastic-viscoplastic field on the plastic yield surface, where the deformations are elastic, plastic and viscoplastic, $\dot{\varepsilon}_{ij} = \dot{\varepsilon}^e_{ij} + \dot{\varepsilon}^p_{ij} + \dot{\varepsilon}^{vp}_{ij}$.

The plastic yield surface $f_p = 0$ is defined in the $q - p$ stress plane by using the Drucker-Prager's criterion (Fig. 2):

$$f_p = q - \alpha_p \cdot p - k_p \quad \text{for} \quad p \geq \sigma_t \tag{2}$$

where α_p and k_p are respectively the slope and the intercept with the q-axis and σ_t is the volumetric tension cut-off.

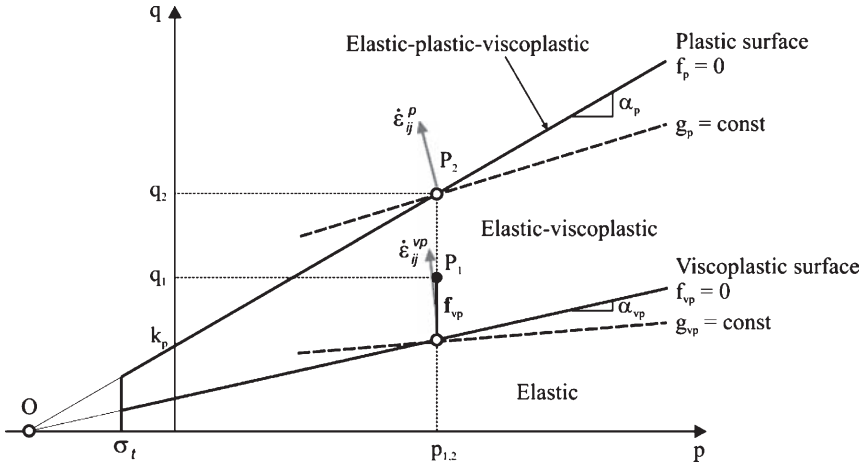

Fig. 2. Limit surfaces and stress fields in the q–p plane

In the current version of the SHELVIP model the plastic yield surface is fixed and cannot harden or soften, neither for the development of plastic strains, nor for the development of viscoplastic strains or versus time.

The viscoplastic yield surface $f_{vp} = 0$ is internal to the plastic yield surface and is defined by using the Drucker-Prager's criterion. This is assumed to intersect the p-axis at the same point (point O in Fig. 2) as the plastic yield surface and to be characterized by the same volumetric tension cut-off σ_t. These assumptions allow to have two homothetic yield surfaces and to reduce the overall number of constitutive parameters. The viscoplastic yield surface can be expressed as:

$$f_{vp} = q - \alpha_{vp} \cdot \left(p + \frac{k_p}{\alpha_p} \right) \quad \text{for} \quad p \geq \sigma_t \tag{3}$$

where α_{vp} defines the slope of the linear criterion.

In order to allow for the threshold for development of viscoplastic strains to change depending on the previous stress history, the viscoplastic yield surface is assumed to harden, by means of the increase of the parameter α_{vp}, as discussed in the following. As a consequence, the parameter α_{vp} can be considered as an internal state parameter of the viscoplastic hardening level of the material (i.e. it is not a true constitutive parameter of the model).

The elastic strain rate component $\dot{\varepsilon}^e_{ij}$ given by Eq. (1), which is always present, can be evaluated directly from the stress rate tensor $\dot{\sigma}_{kl}$ by using a linear elastic law:

$$\dot{\varepsilon}^e_{ij} = C_{ijkl} \cdot \dot{\sigma}_{kl} \tag{4}$$

where C_{ijkl} is the compliance matrix, which is constant and is defined by using the Young's modulus E and the Poisson's ratio υ as follows:

$$C_{ijkl} = \frac{1}{E} \cdot \left[(1 + \upsilon) \cdot \delta_{ik} \cdot \delta_{jl} - \upsilon \cdot \delta_{ij} \cdot \delta_{kl} \right] \tag{5}$$

If the current state of stress is represented by a point on the plastic yield surface (i.e. $f_p(\sigma_{ij}) = 0$), plastic deformations develop and the plastic strain rate tensor $\dot{\varepsilon}_{ij}^{p}$ can be determined by using the classical flow rule of the theory of elastoplasticity:

$$\dot{\varepsilon}_{ij}^{p} = \lambda \cdot \frac{\partial g_p}{\partial \sigma_{ij}} \tag{6}$$

where λ is the so-called plastic multiplier, which can be determined by using the consistency conditions (i.e. during plastic flow $f_p = 0$ and $\dot{f}_p = 0$), and g_p is the plastic potential function that defines the direction of the plastic strain rate tensor.

The plastic flow is non-associated and the plastic potential function g_p is assumed to be a linear function of the deviatoric stress q and of the volumetric stress p as follows:

$$g_p = q - \omega_p \cdot p \tag{7}$$

where ω_p is the plastic dilatancy, which defines the ratio of volumetric to deviatoric plastic strain increments. Only if volumetric tensile yielding occurs the plastic flow is associated and the plastic potential function is equal to the plastic yield function $g_p = f_p$.

If the state of stress exceeds the viscoplastic yield surface (i.e. $f_{vp}(\sigma_{ij}) > 0$), viscoplastic deformations develop. The viscoplastic strain rate tensor $\dot{\varepsilon}_{ij}^{vp}$ can be evaluated by using the flow rule of the overstress theory of Perzyna:

$$\dot{\varepsilon}_{ij}^{vp} = \gamma \cdot \Phi(F) \cdot \frac{\partial g_{vp}}{\partial \sigma_{ij}} \tag{8}$$

where γ is the fluidity parameter, which controls the amplitude of the viscoplastic strain rate, $\Phi(F)$ is the so-called viscoplastic nucleus, F is the overstress function and g_{vp} is the viscoplastic potential function.

It is noted that the overstress function F represents the state of overstress inside the material with respect to a ''static'' condition, which is defined by the viscoplastic yield surface. It quantifies the distance between the stress point and the viscoplastic yield surface. In the SHELVIP model the overstress function is assumed to be equal to the viscoplastic yield function:

$$F = f_{vp} \tag{9}$$

and defines the deviatoric state of stress which exceeds the viscoplastic yield surface.

The viscoplastic nucleus $\Phi(F)$ controls the magnitude of the viscoplastic strain rate. It is assumed to be a power function of the overstress function F:

$$\Phi(F) = \langle F \rangle^n \tag{10}$$

where n is a constitutive parameter ($n > 0$). The Macaulay brackets $\langle\ \rangle$ ($\langle x \rangle = 0$ if $x < 0$ and $\langle x \rangle = x$ if $x \geq 0$) allow for viscoplastic deformations only if the stress point is external to the viscoplastic yield surface.

The viscoplastic potential function g_{vp} defines the direction of the viscoplastic strain rate tensor. It is assumed to be a linear function of the deviatoric stress q and of the volumetric stress p:

$$g_{vp} = q - \omega_{vp} \cdot p \tag{11}$$

where ω_{vp} is the plastic dilatancy, which quantifies the ratio between the volumetric and the deviatoric viscoplastic strain increment.

With the assumptions above and given that:

$$\frac{\partial q}{\partial \sigma_{ij}} = \frac{3}{2} \cdot \frac{s_{ij}}{q} \quad \text{and} \quad \frac{\partial p}{\partial \sigma_{ij}} = \frac{1}{3} \cdot \delta_{ij} \tag{12}$$

Equation (8), which controls the evolution of viscoplastic strain rate, can be rewritten as:

$$\dot{\varepsilon}_{ij}^{vp} = \gamma \cdot f_{vp}^{n} \cdot \left(\frac{3}{2} \cdot \frac{s_{ij}}{q} - \frac{1}{3} \cdot \omega_{vp} \cdot \delta_{ij} \right) \tag{13}$$

In order to complete the formulation of the model, one is to define the hardening law of the viscoplastic yield function. It is of course the most important component and the most significant element of novelty of the SHELVIP model.

The hardening law in nearly all the presently available viscoplastic models is assumed to be controlled by viscoplastic strains, by means of scalar quantities, such as the deviatoric viscoplastic strain ε_q^{vp} or the viscoplastic work W^{vp}, which however are not easily determined from laboratory or in-situ tests. Moreover, these quantities are referred to the initial time t_0 and, as a consequence, cannot be rigorously considered as true state variables of the material.

In order to overcome these limitations a stress based hardening law is introduced. A differential relationship between the time derivative of the parameter α_{vp}, which defines the hardening level of the viscoplastic yield surface, and the state of stress $f_{vp}(\sigma_{ij})$ that exceeds the viscoplastic yield surface is assumed. The proposed hardening law can be written as:

$$\dot{\alpha}_{vp} = \frac{l}{m \cdot n} \cdot \frac{f_{vp}}{p + \dfrac{k_p}{\alpha_p}} \cdot \left(\frac{f_{vp}}{q} \right)^{m \cdot n} \tag{14}$$

where l and m are constitutive parameters ($l > 0$ and $m > 0$).

This is like to state that the existence of a deviatoric state of overstress inside the material for a finite period of time leads to a fixed variation of the viscoplastic yield function, which depends on the overall state of stress defined by q and p.

Equation (14) is apparently complex. However, with the overstress theory of Perzyna holding true, the hardening law of the viscoplastic yield function drives at the same time the evolution of the viscoplastic strains versus time and the evolution of the stress levels for onset of viscoplastic deformations. The physical meaning of the proposed equation becomes self-evident if consideration is given to creep behaviour as discussed below (Section 3).

The introduction of a stress based hardening law is associated with some advantages. The most important one is the possible evaluation of the viscoplastic hardening level of the material from the stress level which defines the threshold for development of viscoplastic deformations, which can be done by appropriate tests. A second one is a clear definition of each time-dependent feature by means of a single constitutive parameter. However, a disadvantage is found in the need to introduce an additional

Table 1. Constitutive parameters of the SHELVIP model

Elastic	E	Young's modulus
	ν	Poisson's ratio
Plastic	α_p	slope of the Drucker-Prager's plastic yield criterion
	k_p	intercept of the Drucker-Prager's plastic yield criterion
	σ_t	volumetric tension cut-off
	ω_p	plastic dilatancy
Viscoplastic	γ	fluidity parameter
	m	shape factor
	n	load dependency factor
	l	time stretching factor
	ω_{vp}	viscoplastic dilatancy

parameter (l) in order to satisfy the dimensional equality between the two terms of Eq. (14).

Considering the viscoplastic law given by Eq. (13) and the hardening law of Eq. (14), it is possible to state that the parameter α_{vp} summarizes by itself all the previous loading history of the material.

With these assumptions holding true, the overall number of constitutive parameters of the SHELVIP model are 11 as summarised in Table 1: 2 classical elastic parameters, 4 classical plastic parameters and 5 viscoplastic parameters. It is a rather limited number, if the introduction of the time variable and the complexity of the model are taken into account.

3. Analytical closed-form solution for creep

If creep conditions are considered, an analytical closed-form solution can be derived from the differential equations of the SHELVIP model. This is important as the constitutive parameters can be determined by using this solution and the experimental results from laboratory creep tests. Also, in this way a better understanding of this model of behaviour can be achieved.

Consider a triaxial creep test characterized by a constant axial stress σ_a and a constant radial stress σ_r, which define a point in the $q - p$ stress plane ($q = \sigma_a - \sigma_r$, $p = (\sigma_a + 2\sigma_r)/3$) located between the viscoplastic yield surface and the plastic yield surface. With this holding true, the behaviour of the material is elasto-viscoplastic.

If the time derivative of the viscoplastic function given by Eq. (3) is introduced into Eq. (14), the hardening law of the viscoplastic yield surface can be rewritten as:

$$\dot{f}_{vp} = -\frac{l}{m \cdot n} \cdot f_{vp} \cdot \left(\frac{f_{vp}}{q}\right)^{m \cdot n} \tag{15}$$

For small intervals of time, the decrease of the state of overstress inside the material, which is caused by the hardening of the viscoplastic yield surface, is directly proportional to the state of overstress itself multiplied by a factor, which

takes into account the ratio between the state of overstress and the overall deviatoric state of stress.

Equation (15) can be easily integrated, leading to:

$$f_{vp} = q \cdot \left[l \cdot t + \left(\frac{q}{f_{vp,0}} \right)^{m \cdot n} \right]^{-\frac{1}{m \cdot n}} \tag{16}$$

where $f_{vp,0}$ is the initial value of the viscoplastic function, given by Eq. (3), with the initial viscoplastic hardening level equal to $\alpha_{vp,0}$.

If Eq. (16) is introduced into Eq. (13), it is possible to derive the axial viscoplastic strain rate $\dot{\varepsilon}_a^{vp}$ in analytical form as follows:

$$\dot{\varepsilon}_a^{vp} = \gamma \cdot q^n \cdot \left[l \cdot t + \left(\frac{q}{f_{vp,0}} \right)^{m \cdot n} \right]^{-\frac{1}{m}} \cdot \left(1 - \frac{\omega_{vp}}{3} \right) \tag{17}$$

The integration of Eq. (17) over time allows one to obtain the following relations for the axial viscoplastic strain ε_a^{vp}:

$$\begin{cases} \varepsilon_a^{vp} = \dfrac{\gamma}{l} \cdot \dfrac{m}{m-1} \cdot q^n \cdot \left\{ \left[l \cdot t + \left(\dfrac{q}{f_{vp,0}} \right)^{m \cdot n} \right]^{\frac{m-1}{m}} - \left(\dfrac{q}{f_{vp,0}} \right)^{n(m-1)} \right\} \cdot \left(1 - \dfrac{\omega_{vp}}{3} \right) & \text{for } m \neq 1 \\ \varepsilon_a^{vp} = \dfrac{\gamma}{l} \cdot q^n \cdot \ln \left[1 + l \cdot t \cdot \left(\dfrac{q}{f_{vp,0}} \right)^{-n} \right] \cdot \left(1 - \dfrac{\omega_{vp}}{3} \right) & \text{for } m = 1 \end{cases} \tag{18}$$

Equations (17) and (18) lead to underline some of the most relevant behavioural features of the SHELVIP model as discussed in the following.

3.1 Strain-time behaviour

Based on Eq. (18), the SHELVIP model incorporates for $m = 1$ the semi-logarithmic law of creep:

$$\varepsilon_a^{vp} = C_\alpha \cdot \ln \left[1 + \frac{t}{t_0} \right] \quad \text{with:} \quad t_0 = \frac{1}{l} \cdot \left(\frac{q}{f_{vp,0}} \right)^n, \quad C_\alpha = \frac{\gamma}{l} \cdot q^n \cdot \left(1 - \frac{\omega_{vp}}{3} \right) \tag{19}$$

where t_0 is the reference time and C_α is the secondary compression coefficient for triaxial creep tests.

The model can correctly take into account the dependency of the reference time t_0 from the loading history of the material. If the initial hardening level $\alpha_{vp,0}$ is equal to zero (i.e. the material did not experience any creep process in the past) the reference time is equal to the inverse of l; otherwise creep strains develop at a lower rate. This allows one to correctly represent a creep process which has started in the past. Furthermore, the model can describe the dependency of the secondary compression coefficient C_α from the applied deviatoric stress q, by means of the constitutive parameter n.

The existence of a different solution for creep strain for $m = 1$ suggests that this particular value should be considered as a critical value that separates two different

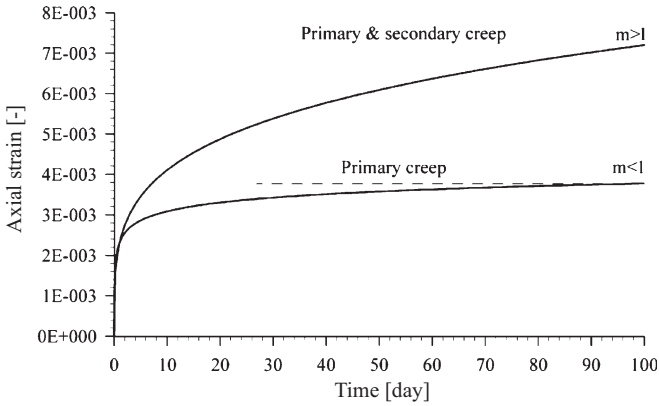

Fig. 3. Creep test. Different behaviour depending on the value of m

models of behaviour. If the limit of the axial viscoplastic strain ε_a^{vp} for time tending to infinity is evaluated, it is possible to obtain:

$$\begin{cases} \lim\limits_{t\to\infty} \varepsilon_a^{vp} = \dfrac{\gamma}{l} \cdot \dfrac{m}{m-1} \cdot \dfrac{q^{n+1}}{f_{vp,0}} \cdot \left(1 - \dfrac{\omega_{vp}}{3}\right) & \text{for} \quad m < 1 \\ \lim\limits_{t\to\infty} \varepsilon_a^{vp} = \infty & \text{for} \quad m \geq 1 \end{cases} \tag{20}$$

If $m < 1$ the axial viscoplastic strain tends to a constant value for time tending to infinity. Therefore the model is able to describe only the primary phase of creep (Fig. 3). If $m > 1$ the axial viscoplastic strain tends to infinity and the model can describe also the secondary phase of creep (Fig. 3).

Rigorously, only the condition $m < 1$ can be considered as physically admissible, because strain cannot exceed the limit of 100% in compression. However, the case $m \geq 1$ can better describe the short-term and the medium-term behaviour. On the contrary, if the long-term behaviour is considered, the condition $m < 1$ will be strictly required.

3.2 Strain rate – time behaviour

If the attention is posed on Eq. (17), which describes the strain rate – time behaviour of the SHELVIP model in a creep test, the typical creep curve plotted in a bi-logarithmic diagram is obtained as shown in Fig. 4. This behaviour is characterized by two different asymptotes, one horizontal on the left (called ''short-time asymptote'') and one inclined on the right (called ''long-time asymptote''), which are joined one to the other one by a curved line.

The limit of the viscoplastic strain rate for time tending to zero is equal to a constant value, and gives the horizontal asymptote on the left:

$$\lim_{t\to 0} \dot{\varepsilon}_a^{vp} = \dot{\varepsilon}_a^{vp}\big|_0 = \gamma \cdot f_{vp,0}^n \cdot \left(1 - \frac{\omega_{vp}}{3}\right) \tag{21}$$

which is shown to considerably improve the numerical stability and the accuracy of the constitutive model. It prevents the strain rate to tend to infinity for time tending

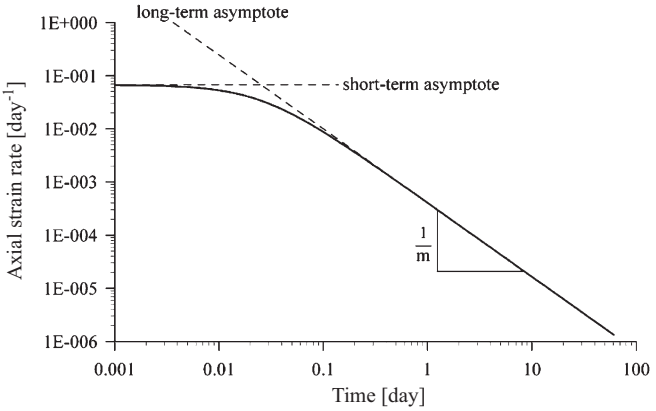

Fig. 4. Creep test. Strain rate-time behaviour

to zero, which is a common problem of full-logarithmic models. Although this asymptote is not clearly evidenced from results of testing, it does not influence significantly the shape of the creep curves, because it involves only the very first instants of time.

The limit of the viscoplastic strain rate for time tending to infinity gives the inclined asymptote on the right:

$$\lim_{t\to\infty} \dot{\varepsilon}_a^{vp} = \dot{\varepsilon}_a^{vp}\big|_{\infty} = \gamma \cdot l^{-\frac{1}{m}} \cdot t^{-\frac{1}{m}} \cdot q^n \cdot \left(1 - \frac{\omega_{vp}}{3}\right) \tag{22}$$

which can be rewritten into logarithmic form as follows:

$$\log\left(\dot{\varepsilon}_a^{vp}|_{\infty}\right) = -\frac{1}{m} \cdot \log(t) + n \cdot \log(q) + \log\left[\gamma \cdot l^{-\frac{1}{m}} \cdot \left(1 - \frac{\omega_{vp}}{3}\right)\right] \tag{23}$$

Thus a linear relationship between the logarithm of viscoplastic strain rate and the logarithm of time, with a slope equal to $1/m$, is obtained as shown in Fig. 4. The SHELVIP model is found to reproduce satisfactorily the results of tests reported by different authors (Singh and Mitchell, 1968; Bishop and Lovenbury, 1969; Tavenas et al., 1978; D'Elia, 1991), except for very small values of time. In fact, these tests exhibit a linear relationship between creep strain rate and time into a logarithmic diagram, when tertiary creep is not present. It is important to observe that the parameter m of the SHELVIP model is equal to the inverse of the parameter m defined by Singh and Mitchell (1968).

It is noted that an equation similar to Eq. (23) can also be obtained for the radial viscoplastic strain rate $\dot{\varepsilon}_r^{vp}$, so that one may state that the parameter m characterises at the same time the evolution of both the volumetric and the deviatoric creep strains as assumed by Tavenas et al. (1978). This applies to the majority of geomaterials, although in cases it may not hold true as reported by Feda (1992) and Tian et al. (1994).

In the SHELVIP model the parameter m is independent from the applied deviatoric stress, as shown by Tavenas et al. (1978) and by den Haan (1994). However, some authors report that m is not always independent from the deviatoric stress: in some

cases m is found to decrease (Bishop and Lovenbury, 1969; Feda, 1992; Tian et al., 1994); in other cases the opposite is true (Zhu et al., 1999). Given this uncertainty, the assumption that m is independent from the deviatoric stress may be acceptable.

3.3 Stress dependency

If the initial viscoplastic hardening level $\alpha_{vp,0}$ is assumed to be equal to zero, the initial value of the viscoplastic overstress function $f_{vp,0}$ is equal to the deviatoric stress q (Eq. (3)) and the equation of the axial viscoplastic strain rate (Eq. (17)) can be rewritten as:

$$\dot{\varepsilon}_a^{vp} = \gamma \cdot q^n \cdot (l \cdot t + 1)^{-\frac{1}{m}} \cdot \left(1 - \frac{\omega_{vp}}{3}\right) \tag{24}$$

It is noted that the viscoplastic strain rate and, as a consequence, the viscoplastic strain given in such a condition by the SHELVIP model depend only on the deviatoric stress q. Then the volumetric stress p does not influence the development of viscoplastic deformations. This particular aspect of the time dependent behaviour is commonly accepted and confirmed by various tests.

According to Eq. (24), a linear relationship exists between the logarithm of the viscoplastic strain rate $\dot{\varepsilon}_a^{vp}$ and the logarithm of deviatoric stress q with a slope equal to the constitutive parameter n. As shown by Mitchell (1993), this relationship describes correctly the stress dependency for the majority of geomaterials below the onset of tertiary behaviour. Above this level the viscoplastic strain rate increases at a greater rate as failure is approached.

3.4 Initial viscoplastic hardening level

It is of interest to analyse the effect of the initial viscoplastic hardening level $\alpha_{vp,0}$ on both the viscoplastic strain rate and the viscoplastic strain during a creep test. To this purpose Eq. (17) can be rewritten as:

$$\dot{\varepsilon}_a^{vp} = \gamma \cdot \left[q \cdot \left(\frac{f_{vp,0}}{q}\right)\right]^n \cdot \left[\left(\frac{f_{vp,0}}{q}\right)^{m \cdot n} \cdot l \cdot t + 1\right]^{-\frac{1}{m}} \cdot \left(1 - \frac{\omega_{vp}}{3}\right) \tag{25}$$

The increase of the initial viscoplastic hardening level $\alpha_{vp,0}$ causes the initial overstress function $f_{vp,0}$ to decrease according to Eq. (3). This leads to two important consequences, as observed by comparing Eqs. (24) and (25). The first consequence is that the viscoplastic strain rate depends on the deviatoric stress q, which is reduced by a factor $(f_{vp,0}/q)$ smaller than 1, if compared to the case of initial viscoplastic hardening equal to zero. The second consequence is that the time t is multiplied now by a factor $(f_{vp,0}/q)^{m \cdot n}$, which is smaller than 1. This implies that the change in viscoplastic strain takes place at a lower rate with respect to the case of initial viscoplastic hardening equal to zero.

If the logarithm of the viscoplastic strain rate is plotted versus the logarithm of time, the increase of the initial overstress level $\alpha_{vp,0}$ is observed to cause the short-term asymptote (Eq. (21)) to move downwards without influencing the long-term asymptote (Eq. (23)), as depicted in Fig. 5. This means that the increase of the initial

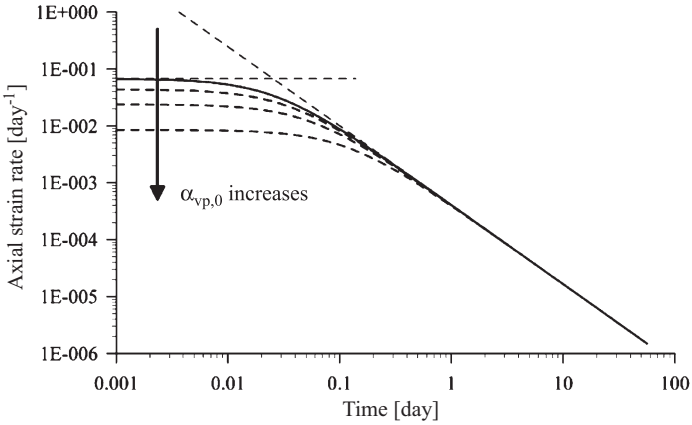

Fig. 5. Creep test. Effect of the initial viscoplastic hardening on the strain rate-time behaviour

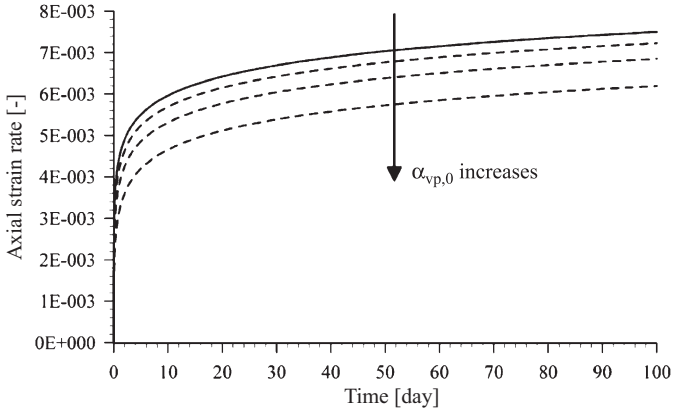

Fig. 6. Creep test. Effect of the initial viscoplastic hardening to the creep curves

viscoplastic hardening level $\alpha_{vp,0}$ influences only the short-term behaviour, and not the long-term behaviour, which is controlled by the deviatoric stress q.

The effect of an increase in the initial viscoplastic hardening level $\alpha_{vp,0}$ on the viscoplastic strain – time response is to bring the creep curves down, as illustrated in Fig. 6. Thus, the magnitude of creep is reduced, but the shape of the curves remain nearly the same.

4. Solution for constant strain rate

An analytical closed form solution of the SHELVIP model for constant strain rate cannot be found. However, in order to highlight the ability of the model to describe the time-dependent behaviour of geomaterials in such a condition, the results of numerical solutions can be considered. To this end, let us take a triaxial constant strain rate test. Assume that, following initial loading to a stress state represented by a point in the $q - p$

plane between the viscoplastic and the plastic yield surfaces, the axial stress σ_a is increased under a constant axial strain rate $\dot{\varepsilon}_a$ as the confining pressure σ_r is kept constant.

For a final stress state below the plastic yield surface, the relationship between the axial strain rate and the axial and radial stresses can be expressed, by using Eqs. (1), (3), (4) and (13), as:

$$\dot{\varepsilon}_a = \frac{\dot{\sigma}_a}{E} + \gamma \left[\sigma_a - \sigma_r - \alpha_{vp} \left(\frac{1}{3}\sigma_a + \frac{2}{3}\sigma_r + \frac{k_p}{\alpha_p} \right) \right]^n \left(1 - \frac{\omega_{vp}}{3} \right) \tag{26}$$

which can be solved numerically with Euler explicit method, if a constant and sufficiently small time step Δt is adopted:

$$\sigma_a^{(t+\Delta t)} = \sigma_a^{(t)} + E \left\{ \dot{\varepsilon}_a - \gamma \left[\sigma_a^{(t)} - \sigma_r - \alpha_{vp}^{(t)} \left(\frac{1}{3}\sigma_a^{(t)} + \frac{2}{3}\sigma_r + \frac{k_p}{\alpha_p} \right) \right]^n \left(1 - \frac{\omega_{vp}}{3} \right) \right\} \Delta t \tag{27}$$

In a similar manner, the evolution of the viscoplastic hardening level α_{vp} can be calculated from Eq. (14) as:

$$\alpha_{vp}^{(t+\Delta t)} = \alpha_{vp}^{(t)} + \frac{l}{m \cdot n} \cdot \frac{1}{\frac{1}{3}\sigma_a^{(t)} + \frac{2}{3}\sigma_r + \frac{k_p}{\alpha_p}} \cdot \frac{\left[\sigma_a^{(t)} - \sigma_r - \alpha_{vp}^{(t)} \left(\frac{1}{3}\sigma_a^{(t)} + \frac{2}{3}\sigma_r + \frac{k_p}{\alpha_p} \right) \right]^{m \cdot n + 1}}{\left(\sigma_a^{(t)} - \sigma_r \right)^{m \cdot n}} \Delta t \tag{28}$$

Equations (27) and (28) allow to determine the axial stress $\sigma_a^{(t)}$ for each time t, starting from the initial values of the axial stress $\sigma_a^{(0)}$ and the viscoplastic hardening level $\alpha_{vp}^{(0)}$. The computation can be performed by using an electronic spreadsheet.

4.1 Triaxial constant strain rate test

Let us consider a series of triaxial constant strain rate tests, performed under the same conditions, but characterized by different values of the axial strain rate $\dot{\varepsilon}_a$. For each test the stress–strain curve can be determined by applying Eqs. (27) and (28), as shown in Fig. 7.

Each curve exhibits a strongly non-linear behaviour below the plastic yield limit. The stiffness of the material decreases as the applied stress increases. This behaviour, which is typical of weak rocks and soils, is usually taken into account in elastoplasticity by using a non linear elastic relationship. On the contrary, the SHELVIP model, like most of time-dependent constitutive laws, can describe this behaviour as an effect of the development of viscoplastic strains.

As illustrated in Fig. 7, in the current version of the SHELVIP model, the material is assumed to be perfectly plastic. However, a hardening or softening post-peak behaviour could be easily taken into account, by defining the dependency of the plastic yield surface from plastic strains. This can be done by changing simultaneously α_p and k_p, in order to maintain the ratio k_p/α_p constant. This allows not to change the intersect of the plastic yield surface with the p-axis, without influencing the viscoplastic yield surface, which is defined by Eq. (3).

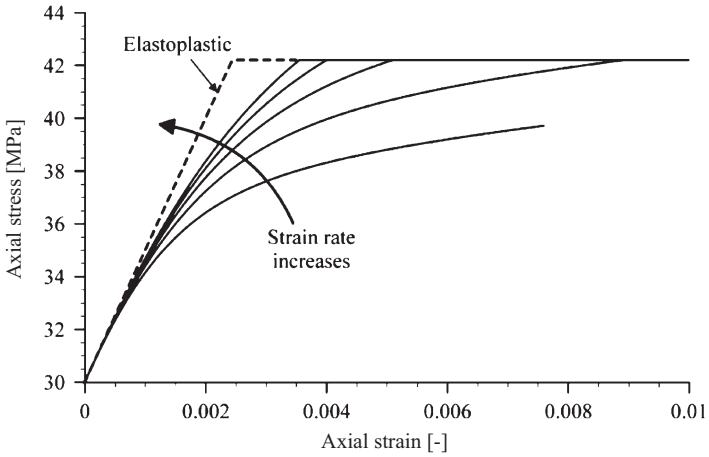

Fig. 7. Constant strain rate test. Stress–strain curves obtained for different values of the applied axial strain rate

According to the typical behaviour of weak rocks and soils, the stiffness increases as the applied strain rate increases. On the contrary, the peak strength is constant and does not depend on the level of the applied rate of strain. This is not supported by the results of testing, which instead highlight an increase of the peak strength with the increase of the applied strain rate (Tavenas et al., 1978; Vaid et al., 1979; Zhu et al., 1999). This behaviour is essentially due to the fact that, in the current version of the SHELVIP model, the plastic yield surface is fixed and cannot change position neither by means of the viscoplastic strains, nor by means of time. This limit will be removed in future improvements of the model, by introducing a viscoplastic hardening of the plastic yield surface.

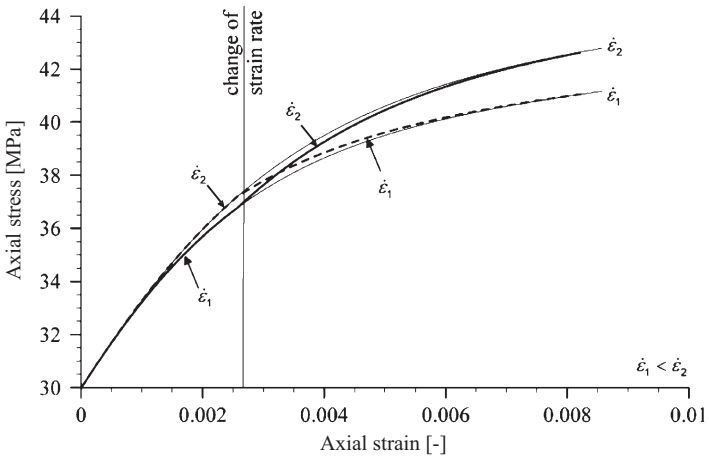

Fig. 8. Constant strain rate test. Effect of change of applied axial strain rate

If the axial strain rate tends to infinity (i.e. it is sufficiently large) the behaviour of the material is purely linear elastic as illustrated in Fig. 7. According to the assumptions of the SHELVIP model, the linearity or the non linearity is not an intrinsic property of the material but depends on the level of the applied strain rate.

Consider now a stress point located exactly on the viscoplastic yield surface. If the axial strain rate tends to zero, the increase of the axial stress tends to zero, and, as a consequence, the stress–strain curve tends to be horizontal. This is not in agreement with the existence of a ''static stress–strain curve'' as postulated by some authors (Vaid and Campanella, 1977; Sulem, 1983).

Finally, it is of interest to analyse the effect of a change of the applied axial strain rate during a constant strain rate test. As depicted in Fig. 8, if the axial strain rate is changed from a value to another one, the stress–strain curve gradually moves according to the ''isotach behaviour'', so that a unique relationship exists between stress, strain and strain rate.

4.2 Triaxial stress relaxation test

A triaxial stress relaxation test can be considered equivalent to a constant strain rate test with the applied axial strain rate $\dot{\varepsilon}_a$ equal to zero. If the starting stress point is located between the viscoplastic and the plastic yield surfaces, Eqs. (27) and (28) can be used to describe a stress relaxation process. Figure 9 shows a typical example of the curve which is obtained.

It is noted that the SHELVIP model can reproduce correctly the stress relaxation behaviour, which is widely described in literature (e.g. Vialov and Skibitsky, 1961; Silvestri et al., 1988; Sheahan et al., 1994). The initial stress rate tends to infinity. Then, the stress rate decreases and tends asymptotically to a value equal to zero. A final relaxed state is therefore reached asymptotically after a certain time.

The existence of a final relaxed stress state, which is based on the experimental work carried out by a number of authors (e.g. Vialov and Skibitsky, 1961; Silvestri

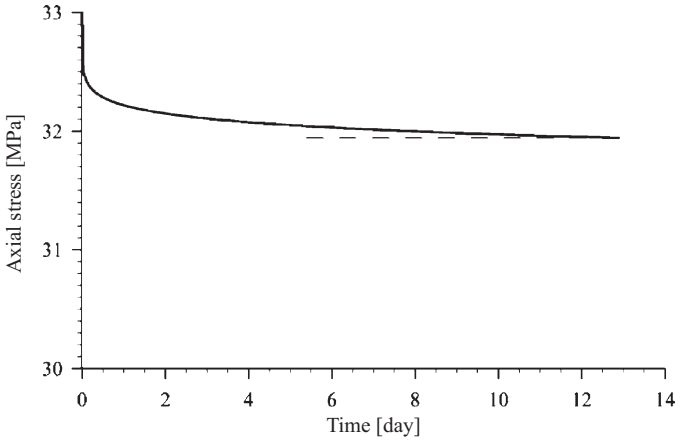

Fig. 9. Stress relaxation test. Decrease of the axial stress versus time

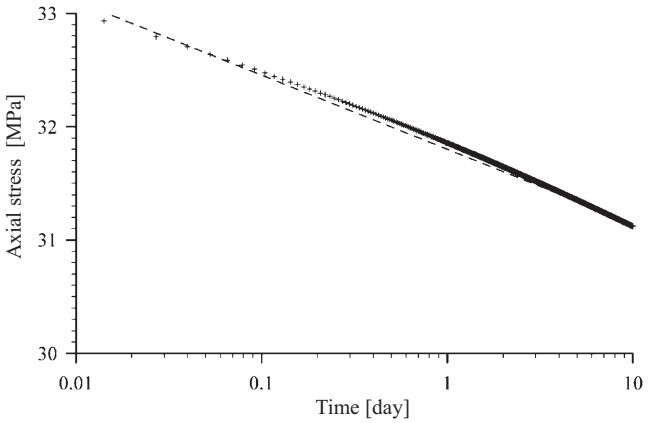

Fig. 10. Stress relaxation test. Decrease of the axial stress versus logarithm of time

et al., 1988; Sheahan et al., 1994; Zhu et al., 1999), is an important feature of the SHELVIP model which has been developed with the intent to catch this particular aspect of the time dependent response.

Finally, if the stress decrease is plotted versus the logarithm of time (Fig. 10), a nearly linear trend can be observed at the intermediate stress level, which confirms the experimental observations reported by Lacerda and Houston (1973).

4.3 Ageing

The effects of ageing are very important for soils and weak rocks, and can be observed in the stress–strain relation subsequent to long periods of creep. The SHELVIP model can reproduce correctly only the accumulated effect which has been defined ''ageing without structuration'' (Tatsouka et al., 2000) or ''apparent preconsolidation effects''. Obviously it cannot take into account the accumulated effects related to a temporary or persistent structuration of the material.

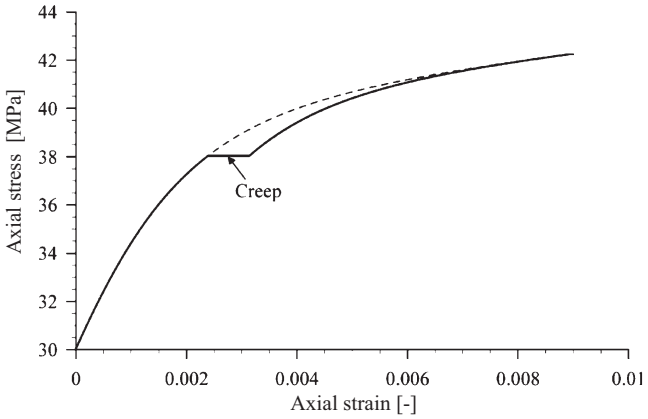

Fig. 11. Ageing. Apparent preconsolidation effect

As shown in Fig. 11, if a material is reloaded after a creep phase, the apparent preconsolidation effect appears. The reloading stress–strain curve starts with a higher stiffness, and, after some time, it reaches again the original compression curve.

5. Calibration of constitutive parameters from creep tests

Following the illustration of the most relevant features of behaviour which characterise the SHELVIP model, the attention is posed on the calibration of constitutive parameters based on the results of laboratory tests. The difficulties associated with such a process usually increase with the increase of the complexity of the model. This holds true for viscoplastic models, which are generally characterized by a large number of constitutive parameters. Also, the identification process is often more difficult by the unclear physical meaning of the constitutive parameters being used.

The calibration process can be performed by means of analytical or semi-analytical fitting, if a closed form solution is available, or by means of numerical optimization fitting, if the complexity of the problem is too high. Analytical fitting allows one to handle the constitutive parameters with more awareness, while numerical fitting is generally faster and more accurate. If possible, one should find a first set of parameters by analytical fitting, subsequently to be refined by a numerical optimization procedure.

In this section the analytical calibration of the constitutive parameters of the SHELVIP model is described with reference to the results of laboratory tests performed on clay shales, a rock formation from the Raticosa tunnel, which experienced very important squeezing problems during excavation (Bonini et al., 2007).

As described in Section 2, the constitutive parameters of the SHELVIP model can be subdivided in three different groups: elastic, plastic, and viscoplastic. Because of the mathematical formulation of the model, the calibration can be performed independently for each group of parameters.

The elastic and plastic parameters are coincident with the elastic and plastic parameters of the classical theory of elastoplasticity, as often used in design

Table 2. Constitutive parameters of the SHELVIP model for clay shales

	Analytical fitting			Numerical fitting		
Elastic	E	50	Mpa	E	50	MPa
	ν	0.3		ν	0.3	
Plastic	α_p	0.607		α_p	0.607	
	k_p	42.34	kPa	k_p	42.34	kPa
	σ_t	−10.00	kPa	σ_t	−10.00	kPa
	ω_p	0		ω_p	0	
Viscoplastic	γ	1.097E-5	*	γ	2.264E-5	*
	m	0.928	*	m	1.005	*
	n	1.411	*	n	1.448	*
	l	30.31	*	l	144.86	*
	ω_{vp}	−0.41		ω_{vp}	−0.41	

* Time in days and pressure in kPa

Table 3. Triaxial creep tests performed on clay shales*

Test	Type	$B(-)$	$b.p.$ (kPa)	σ_c (kPa)	$\dot{\varepsilon}_a$ (mm/min)	$t_{\max}$ (kPa)	s_{const} (kPa)	Δu (kPa)
RTC3	$\text{CIU} + \text{U}_{\text{creep}}$	0.77	399	497	0.005	148	480	18
RTC4	$\text{CIU} + \text{U}_{\text{creep}}$	0.80	404	488	0.005	94	453	31
RTC5	$\text{CIU} + \text{U}_{\text{creep}}$	0.65	396	501	0.001	134	491	9

* B = Skempton's parameter; $b.p.$ = back pressure; σ_c = consolidation effective stress; $\dot{\varepsilon}_a$ = axial strain rate in the shearing phase; $t_{\max} = (\sigma_a - \sigma_r)_{\max}/2$; $s_{\text{const}} = (\sigma_a + \sigma_r)_{\text{const}}/2$; Δu = excess pore pressure

practice. Although there is no need to describe here the calibration procedure used for them, it is important to remember that the elastic modulus should be evaluated from the unloading phase, and the plastic parameters should be determined as peak values.

The elastic and plastic parameters of clay shales are summarised in Table 2. The strength parameters are calculated directly from the Mohr-Coulomb parameters ($c' = 20\,\text{kPa}$, $\phi' = 16^\circ$, $\sigma_t = 5\,\text{kPa}$) by using a circumscribing Drucker-Prager's criterion. The plastic dilatancy is assumed to be equal to zero, in absence of direct measurements.

The identification of the viscoplastic parameters is complex, due to the complexity and generality of the SHELVIP model. At least two triaxial creep tests, performed at different deviatoric stress levels or, alternatively, one triaxial stress relaxation test, are required in order to assess the stress dependency. Radial displacement measurements are necessary to determine the viscoplastic dilatancy.

With the intent to calibrate the viscoplastic parameters of clay shales, three triaxial undrained creep tests (Bonini, 2003; Bonini et al., 2007) performed at different stress levels are considered (Table 3). The main difficulty of these tests is that undrained creep is not rigorously a ''pure creep'', as the variation of pore pressure during the test can modify significantly the effective state of stress inside the specimen. It is important to observe that undrained conditions were in this case strictly required, to prevent the development of swelling deformations, that are significant in clay shales (Bonini, 2003; Bonini et al., 2007). In order to overcome this limitation, the influence of pore pressure is not taken into account and all the creep tests are treated as drained.

The first viscoplastic constitutive parameter, which can be easily determined, is the viscoplastic dilatancy ω_{vp}, which defines the ratio between the volumetric and the deviatoric viscoplastic strain increments:

$$\omega_{vp} = -\frac{\Delta\varepsilon_p^{vp}}{\Delta\varepsilon_q^{vp}} \tag{29}$$

If triaxial conditions are considered, the viscoplastic dilatancy ω_{vp} can be evaluated directly from the ratio between the radial viscoplastic increment $\Delta\varepsilon_r^{vp}$ and the axial viscoplastic strain increment $\Delta\varepsilon_a^{vp}$ as:

$$\omega_{vp} = -\frac{3}{2} \cdot \frac{1 + 2 \cdot \dfrac{\Delta\varepsilon_r^{vp}}{\Delta\varepsilon_a^{vp}}}{1 - \dfrac{\Delta\varepsilon_r^{vp}}{\Delta\varepsilon_a^{vp}}} \tag{30}$$

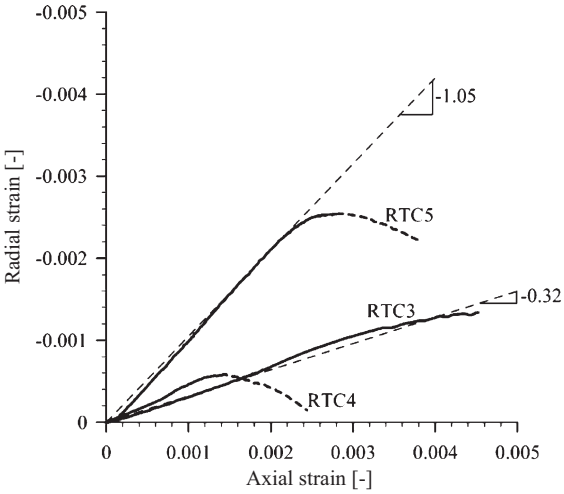

Fig. 12. Radial creep strains versus axial creep strains for the creep test on clay shales

If, for all the creep tests performed on clay shales, the radial strain is plotted versus the axial strain, a non-homogeneous behaviour is observed as illustrated in Fig. 12. Even neglecting the decreasing phases of the radial strain, the ratio between the radial and the axial creep strains are shown to vary between -0.32 and -1.05. The corresponding value of the viscoplastic dilatancy varies between -0.41 and 0.80, with the negative values being associated to a decrease of the volume of the sample and the positive ones to its increase. Neglecting the RTC5 test, which differs significantly from the other two tests, a value of the viscoplastic dilatancy ω_{vp} equal to -0.41 can be assumed (Table 2).

At this point it is necessary to evaluate the initial viscoplastic hardening level $\alpha_{vp,0,i}$ for each creep test i performed. This quantity can be estimated from the stress level $q_{ini,i}$, $p_{ini,i}$, which defines the onset of viscoplastic deformations, by using Eq. (3) and the definition of the viscoplastic yield surface $f_{vp} = 0$:

$$\alpha_{vp,0,i} = \frac{q_{ini,i}}{p_{ini,i} + \dfrac{k_p}{\alpha_p}} \tag{31}$$

If the sample has been subjected for a long time to a constant state of stress, which has never been exceeded in the past, it is reasonable to assume that the time-dependent process is completed, and the stress point is located on the viscoplastic yield surface. Therefore, this state of stress represents the stress threshold for development of viscoplastic deformations q_{ini}, p_{ini}.

From the laboratory tests on clay shales, no experimental evidence of stress thresholds for the development of viscoplastic deformations is available. Also the in-situ state of stress to evaluate these thresholds is not known. Therefore, the initial viscoplastic hardening level $\alpha_{vp,0,i}$ is assumed to be equal to zero for all the creep tests (Table 4). The corresponding values of the initial viscoplastic overstress function $f_{vp,0,i}$ are equal to the deviatoric state of stress q_i (Table 4).

Table 4. Parameters used in the calibration of the creep tests on the clay shales

Test	q_{creep} (kPa)	p'_{creep} (kPa)	$\alpha_{vp,0}$ (−)	$f_{vp,0}$ (kPa)	m (*)	χ (*)	n (*)	θ (*)	γ (*)	l (*)	γ corrected (*)
RTC3	290	430	0	290	0.856	5.960E-4	–	–	1.222E-5	–	1.138E-5
RTC4	178	422	0	178	1.085	3.020E-4	–	–	2.516E-6	–	1.086E-5
RTC5	271	446	0	271	0.841	5.540E-4	–	–	1.110E-5	–	1.068E-5
All	–	–	–	–	0.928	–	1.411	2.010E-7	8.615E-6	30.31	1.097E-5

* Time in days and pressure in kPa

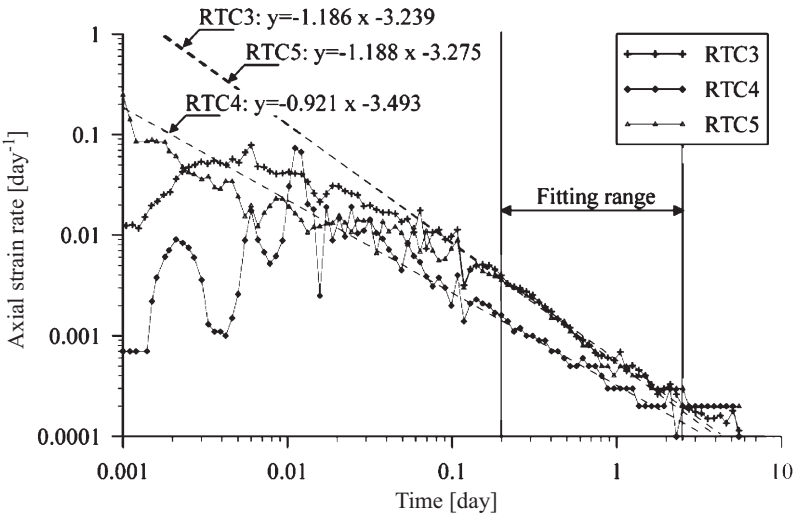

Fig. 13. Axial creep strain rate versus time in a logarithmic diagram for the creep tests on clay shales

To identify the remaining four viscoplastic parameters, only the axial creep strains from triaxial laboratory creep tests are taken into account, as the axial measurements are generally more reliable and accurate than the radial ones. If the logarithm of the axial creep strain rate is plotted versus the logarithm of time, the diagram of Fig. 13 is obtained. Then, a fitting procedure can be applied to the characteristics equations of the SHELVIP model illustrated in Section 3.2, with reference to the existence of the ''short-time asymptote'' and the ''long-time asymptote''.

By using Eq. (23), the parameter m_i can be evaluated for each creep test as the inverse of the slope of the linear interpolation of the experimental data for high values of time t. Figure 13 shows this procedure for the creep tests on clay shales and Table 4 gives the m_i values obtained. The constitutive parameter m is then chosen as the arithmetic mean of all the parameters m_i.

If both terms of Eq. (22) are divided by the quantity $t^{-1/m}$, one obtains:

$$\chi = \frac{\dot{\varepsilon}_a^{vp}\big|_\infty}{t^{-\frac{1}{m}}} = \gamma \cdot l^{-\frac{1}{m}} \cdot q^n \cdot \left(1 - \frac{\omega_{vp}}{3}\right) \tag{32}$$

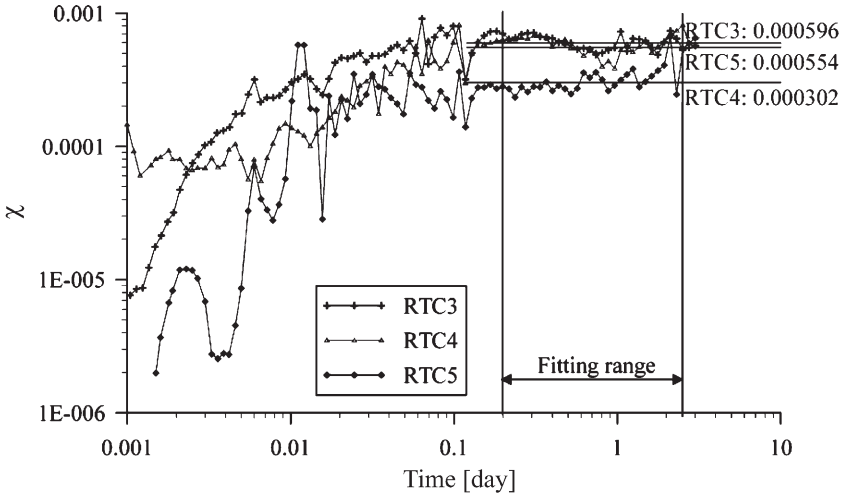

Fig. 14. Procedure for the determination of the parameters χ_i for the creep tests on clay shales

Therefore, as shown in Fig. 14, for each test the axial strain rate divided by $t^{-1/m}$ is plotted versus time into a logarithmic diagram and the quantities χ_i are evaluated as the arithmetic mean of the experimental data, by considering the same fitting range given in Fig. 13. The values of χ_i are shown in Table 4.

Equation (32) can be rewritten into a logarithmic form, to give:

$$\log(\chi) = n \cdot \log(q) + \log(\theta) \quad \text{with} \quad \theta = \gamma \cdot I^{-\frac{1}{m}} \cdot \left(1 - \frac{\omega_{vp}}{3}\right) \tag{33}$$

As illustrated in Fig. 15, the logarithm of the quantities χ_i is plotted versus the logarithm of the deviatoric stresses q_i. Then n and θ can be calculated respectively as the slope and the exponential with base 10 of the intercept with the y-axis of the linear interpolation of the experimental data. The results obtained for n and θ are reported in Table 4.

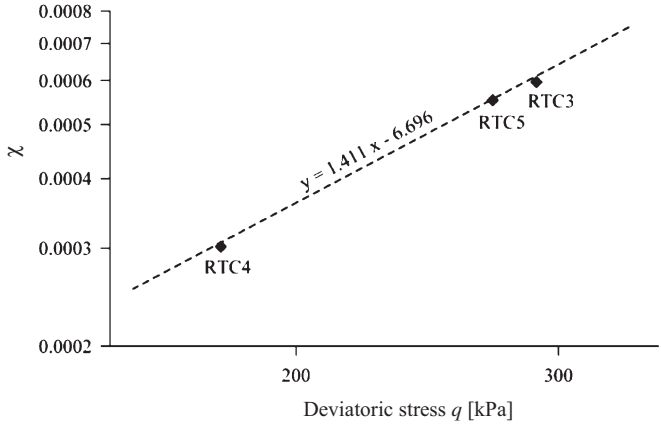

Fig. 15. Procedure for the determination of the parameters n and θ for the creep tests on clay shales

The constitutive parameter γ can be evaluated from the "short-time asymptote" of Eq. (21) as:

$$\gamma = \frac{\dot{\varepsilon}_a^{vp}|_0}{f_{vp,0}^n \cdot \left(1 - \frac{\omega_{vp}}{3}\right)} \tag{34}$$

As shown in Fig. 16, for each creep test the axial strain rate divided by $f_{vp,0,i}^n \cdot (1 - \omega_{vp}/3)$ is plotted versus time into a logarithm diagram. The parameter γ_i is the evaluated for each test as the arithmetic mean of the experimental data for very small values of time t. The values of γ_i are shown in Table 4, where also given is the value of γ as the arithmetic mean of all the γ_i values.

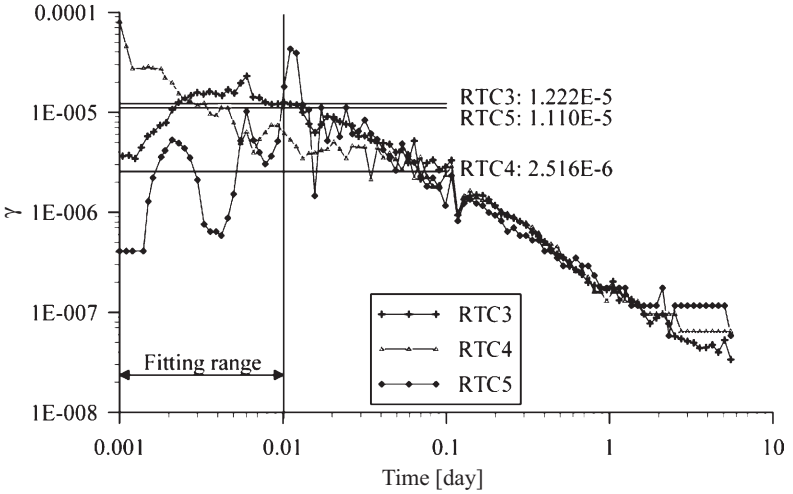

Fig. 16. Procedure for the determination of the parameter γ for the creep tests on clay shales as a first approximation

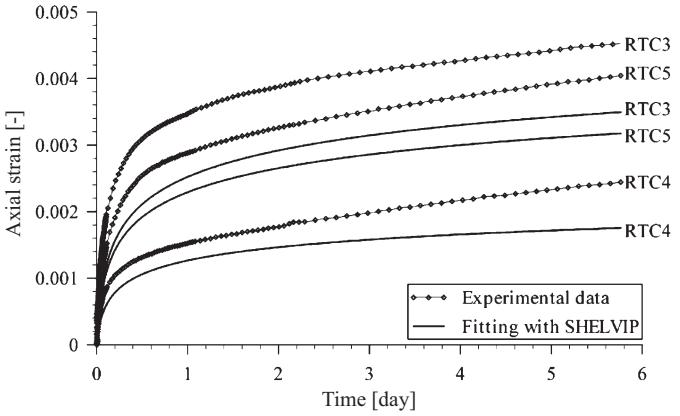

Fig. 17. Comparison of laboratory and modelled creep curves for clay shales, by using the first approximation set of parameters

Finally the remaining parameter l can be calculated from Eq. (33), based on the values of γ and θ:

$$l = \left[\frac{\gamma}{\theta}\cdot\left(1-\frac{\omega_{vp}}{3}\right)\right]^{m} \tag{35}$$

With the values derived for the constitutive parameters given in Table 4, Eq. (18) can be used to compare the computed creep curves with those obtained from triaxial test on clay shales as shown in Fig. 17. This comparison results to be unsatisfactory. This is due to the fact that the calibration has been performed by using the rates of creep strains instead of the creep strains. In order to reduce the discrepancy, the following procedure has been adopted.

The fluidity parameter γ is obtained from Eq. (18) as follows:

$$\gamma = \frac{\varepsilon_a^{vp}}{\tau(t)} \tag{36}$$

where:

$$\begin{cases} \tau(t) = \dfrac{1}{l}\cdot\dfrac{m}{m-1}\cdot q^{n}\cdot\left\{\left[l\cdot t+\left(\dfrac{q}{f_{vp,0}}\right)^{m\cdot n}\right]^{\frac{m-1}{m}}-\left(\dfrac{q}{f_{vp,0}}\right)^{n(m-1)}\right\}\cdot\left(1-\dfrac{\omega_{vp}}{3}\right) & \text{for } m\neq 1 \\ \tau(t) = \dfrac{1}{l}\cdot q^{n}\cdot\ln\left[1+l\cdot t\cdot\left(\dfrac{q}{f_{vp,0}}\right)^{-n}\right]\cdot\left(1-\dfrac{\omega_{vp}}{3}\right) & \text{for } m=1 \end{cases} \tag{37}$$

Then, as shown in Fig. 18, for each creep test the axial strain ε_a^{vp} divided by $\tau(t)$ is plotted versus time. The parameter γ_i can be obtained for each curve as the corresponding arithmetic mean value derived, as given in Table 4. Finally γ is chosen as the arithmetic mean of all the parameters γ_i. Based on the new value of the fluidity parameter γ, the computed and measured creep curves compare extremely well, as illustrated in Fig. 19. Also very satisfactory is the comparison of computed and measured values of creep strain rate versus time as shown in Fig. 20.

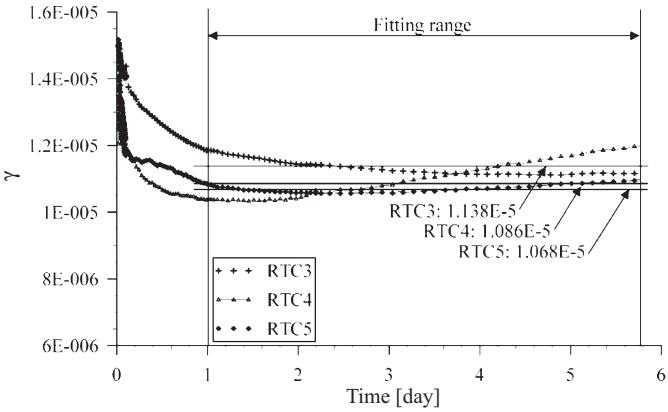

Fig. 18. Procedure for the calibration of the parameters γ_i for the creep tests on clay shales, by using the creep strains

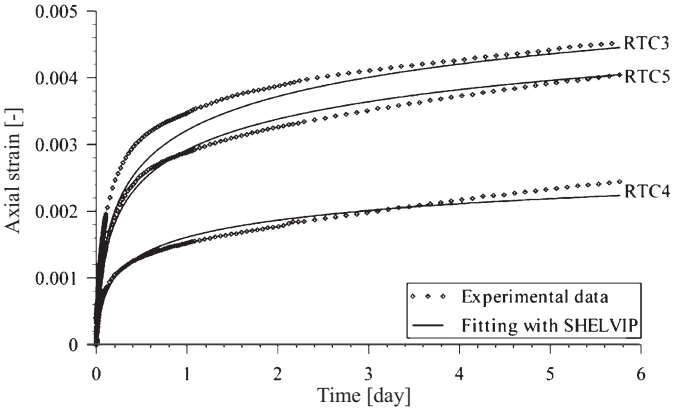

Fig. 19. Comparison of laboratory and modelled creep curves for clay shales, by using the final set of parameters

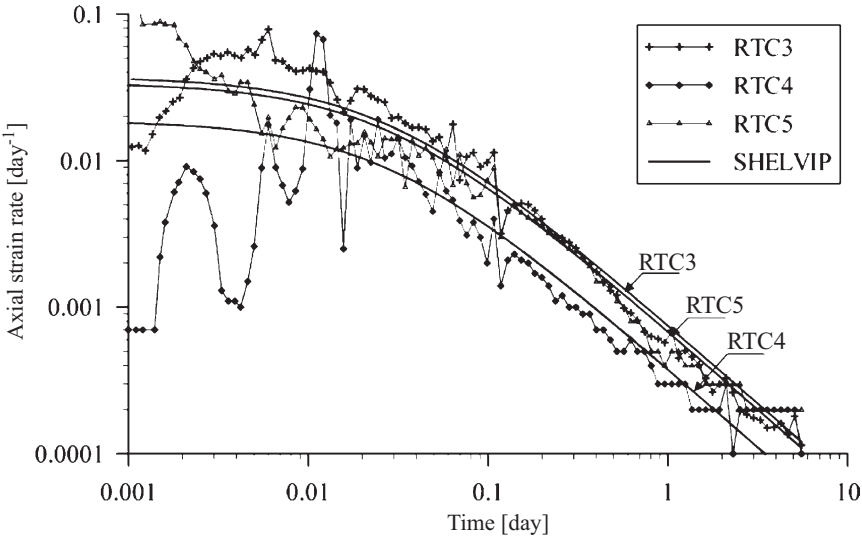

Fig. 20. Comparison of laboratory and modelled strain rate curves for clay shales, by using the final set of parameters

If a numerical optimization fitting procedure is applied to the creep tests available, by using this set of viscoplastic parameters as first-trial values, a new set of parameters is obtained (Table 2). The values of m and n, which define respectively the shape of the creep curves and the load dependency, are very similar to those already available. The values of the parameters γ and l differ more significantly from the previous ones. It is noted that m and n are power of the model, and, therefore, a little change of their values can produce a very important change of both γ and l, which are multiplier coefficients. If the creep curves based on the new parameters

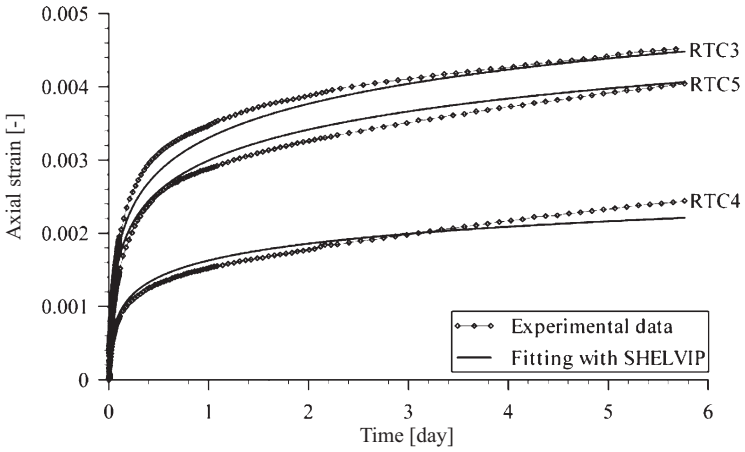

Fig. 21. Comparison of laboratory and modelled creep curves for clay shales, by using the set of parameters determined by numerical fitting

are plotted in Fig. 21, an even better approximation to the laboratory data is obtained.

6. Application to a stress relaxation test

To assess the time-dependent characteristics, triaxial stress relaxation tests are frequently preferred to triaxial creep tests. Relaxation tests require a shorter time for testing (i.e. a relaxation process generally ends faster than a creep process) and in general a small number of tests is needed. However, one may apply this testing procedure provided that the ''correspondence principle'', which states that creep and relaxation are due to the same basic mechanism (Sheahan and Kaliakin, 1999), is assumed to hold true. Also, for most of the viscoplastic models found in literature, a closed-form analytical solution for stress relaxation is not available and a numerical calibration is to be performed.

With the intent to test the ability of the SHELVIP model to describe the stress relaxation process, a triaxial stress relaxation test, carried out on a coal sample taken from the Carboniferous Formation during the excavation of the Saint Martin La Porte access tunnel, is considered in this section (Barla et al., 2007). In this test, which was performed as part of a comprehensive testing program on coal (Debernardi, 2008), following a loading phase with a constant mean stress $s = 20$ MPa and a constant axial stress rate $\dot{\sigma}_a = 0.083$ MPa/min up to the deviatoric stress $t = 13$ MPa, the decrease of the axial stress was measured versus time, as shown in Fig. 22, with the axial strain and the confining pressure kept constant.

The constitutive parameters of the SHELVIP model determined for this test are shown in Table 5. The elastic and plastic parameters were obtained from simple and multi-stage strength tests. The viscoplastic dilatancy was estimated on the basis of simple and multi-stage creep tests with the same procedure described above in Section 5. The remaining four viscoplastic parameters were obtained by fitting the

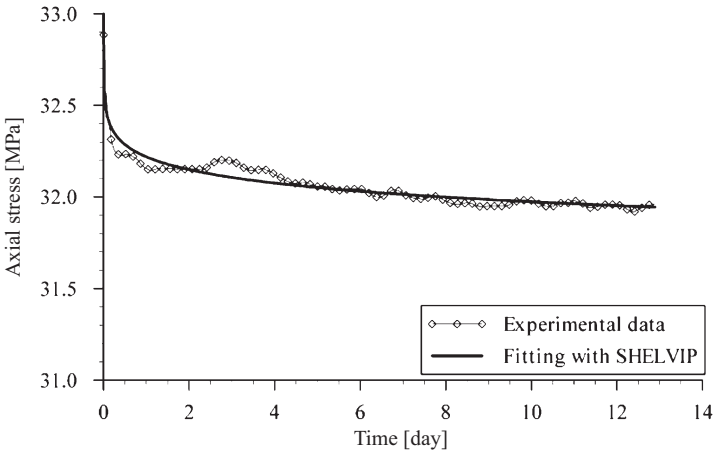

Fig. 22. Comparison of laboratory and modelled triaxial stress relaxation curves on coal

Table 5. Constitutive parameters of the SHELVIP model for the coal

Elastic	E	5000	MPa
	ν	0.3	
Plastic	α_p	1.393	
	k_p	7.16	MPa
	σ_t	−0.10	MPa
	ω_p	0	
Viscoplastic	γ	1.312E-43	*
	m	1.142	*
	n	10.23	*
	l	4.821E + 7	*
	ω_{vp}	0.735	

* Time in days and pressure in kPa

experimental data with the incremental solution of Eqs. (27) and (28) and a numerical optimization procedure. Figure 22 shows a comparison between the experimental data and the numerical solution. The agreement found is excellent.

7. Conclusions

SHELVIP, a new viscoplastic constitutive model, has been developed with the intent to describe the behaviour of rocks in tunnels excavated in very severe squeezing conditions (Barla, 2002). The mathematical formulation of this model has been illustrated in this paper.

This model is shown to couple the general theory of elastoplasticity with a time-dependent component. In the stress space an external non-hardening plastic yield surface defines the locus of plastic strain development, while an internal stress-hardening viscoplastic yield surface establishes the onset of viscoplastic strains. These are not limited to the deviatoric components and are governed by a deviatoric overstress state with respect to the viscoplastic yield surface.

An analytical closed-form solution for triaxial creep conditions has been derived on the basis of the SHELVIP model. It has been shown that this can catch very well nearly all the most important features of the time-dependent behaviour with the exception of the tertiary phase of creep. An incremental numerical solution for triaxial constant strain rate and triaxial stress relaxation conditions has been proposed.

The results of triaxial creep tests performed on clay shales have been used for the selection of the parameters which allow to match the observed behaviour. The analytical calibration used has been discussed in detail together with the fitting by numerical optimization. It is shown that the proposed model gives quite a good match to both the strain versus time and the strain rate versus time curves obtained by laboratory tests for clay shales.

With the intent to underline the generality of the newly developed constitutive model in dealing with the time-dependent behaviour of weak rock and soil, as typically encountered in design analysis of tunnels in squeezing conditions, the application to a triaxial stress relaxation test on a coal sample has been discussed. It can be seen that the model response is again in excellent agreement with the experimental data.

Acknowledgments

This work has been carried out with the financial support of Egis, Antea, Alpina, according to contract No. 5028/06/07 with Politecnico di Torino, Department of Structural and Geotechnical Engineering, which is gratefully acknowledged. Also to be acknowledged is the funding of a post-doctoral fellowship by SiTI, Torino, on behalf of the first author.

References

Barla G (1995) Squeezing rocks in tunnels. ISRM News J II(3–4): 44–49

Barla G (2002) Tunnelling under squeezing rock conditions. In: Kolymbas D (ed) Eurosummer-School in Tunnel Mechanics. Innsbruck 2001, State of the art paper. Logos Verlag, Berlin, pp 169–268

Barla G (2005) Design analysis for tunnels in squeezing rock. Proc. of the 11th International Conference of IACMAG, Torino

Barla G, Barla M, Bonini M, Debernardi D (2007) Lessons learned during the excavation of the Saint Martin La Porte access gallery along the Lyon-Turin base tunnel. BBT 2007, Symposium Brenner Basistunnel uns Zulaufstrecken. Innsbruck University Press, Innsbruck

Bishop AW, Lovenbury HT (1969) Creep characteristics of two undisturbed clays. Proc. 7th ICSMFE, Vol. 1, pp 29–37, Mexico

Bonini M (2003) Mechanical behaviour of clay-shales (argille scagliose) and implications on the design of tunnels. Ph.D. Thesis, Politecnico di Torino, Torino

Bonini M, Debernardi D, Barla M, Barla G (2007) The mechanical behaviour of clay shales and implications on the design of tunnels. Rock Mech Rock Engng 42(2): 361–388

Debernardi D (2008) Viscoplastic behaviour and design of tunnels. Ph.D. Thesis, Politecnico di Torino, Department of Structural and Geotechnical Engineering, Italy

den Haan EJ (1994) Vertical compression of soils. Ph.D. Thesis, Delft university, Department of Civil Engineering and Geosciences, The Netherlands

D'Elia B (1991) Deformation problems in the Italian structurally complex clay soils. 10th European Conf. on Soil Mech. and Found. Engrg., Vol. 4, pp 1159–1170

Feda J (1992) Creep of soils and related phenomena. Development in geotechnical engineering, Vol. 68. Elsevier Science, Amsterdam

Lacerda WA, Houston WN (1973) Stress relaxation in soil. Proc. 8th ICSMFE, Vol. 1, pp 221–227

Mitchell JK (1993) Foundamentals of soil behavior, 2nd edn. John Wiley & Sons, New York

Perzyna P (1966) Foundamental problems in viscoplasticity. Adv Appl Mech 9: 244–377

Sheahan TC, Ladd CC, Germaine JT (1994) Time-dependent triaxial relaxation behavior of a resedimented clay. Geotech Test J 17(4): 444–452

Sheahan TC, Kaliakin VN (1999) Microstructural considerations and validity of the correspondence principle for cohesive soils. In: Jones N, Ghanem R (eds) Engineering Mechanics, Proc. 13th Conf., ASCE, Baltimore, Md.

Silvestri VMS, Touchan Z, Fay B (1988) Triaxial relaxation tests on a soft clay. Advanced triaxial testing of soil and rock, pp 321–337. ASTM, Philadelphia

Singh A, Mitchell JK (1968) General stress-strain-time function for soil. J Soil Mech Found Div 94(1): 21–46

Steiner W (1996) Tunnelling in squeezing rocks: case histories. Rock Mech Rock Engng 29: 211–246

Sulem J (1983) Comportement différé des galeries profondes. Ph.D. Thesis, Ecole Nationale des Pontes et Chaussees

Tatsuoka F, Santucci de Magistris F, Hayano K, Momoya Y, Coseni J (2000) Some new aspects of time effects on the stress-strain behaviour of stiff geomaterials. In: Evangelista R, Picarelli L (eds) The geotechnics of hard soils-soft rocks, Balkema, Rotterdam, The Netherlands, Vol. 2, pp 1285–1371

Tavenas F, Leroueil S, La Rochelle P, Roy M (1978) Creep behaviour of an undisturbed lightly overconsolidated clay. Can Geotech J 15(3): 402–423

Tian WM, Silva AJ, Veyera GE, Sadd MH (1994) Drained creep of undisturbed cohesive marine sediments. Can Geotech J 31: 841–855

Vaid YP, Campanella RG (1977) Time-dependent behavior of undisturbed clay. J Geotech Engng 103(GT7): 693–709

Vaid YP, Robertson PK, Campanella RG (1979) Strain rate behaviour of Saint-Jean-Vianney clay. Can Geotech J 16: 34–42

Vialov SS, Skibitsky AM (1961) Problems of the rheology of soils. Proc. 5th Int. Conf. on Soil Mech. and Found. Engrg., Vol. 1, pp 387–392

Zhu JG, Yin JH, Luk ST (1999) Time-dependent stress-strain behaviour of soft Honk Kong marine deposits. Geotech Test J 22(2): 112–120